

# High Resolution Polarimetry of the Inner Galaxy

Bryan M. Gaensler<sup>1</sup>, J. M. Dickey<sup>2</sup>, N. M. McClure-Griffiths<sup>3</sup>,  
N. S. Bizunok<sup>4</sup>, A. J. Green<sup>5</sup>

<sup>1</sup>*Harvard-Smithsonian Center for Astrophysics, Cambridge MA 02138, USA*

<sup>2</sup>*University of Minnesota, Minnesota MN 55455, USA*

<sup>3</sup>*Australia Telescope National Facility, Epping NSW 1710, Australia*

<sup>4</sup>*Boston University, Boston MA 02215, USA*

<sup>5</sup>*University of Sydney, NSW 2006, Australia*

## Abstract.

We present our results from the Southern Galactic Plane Survey, an effort to map the fourth quadrant of the Milky Way in linear polarization at a frequency of 1.4 GHz and at a resolution of 1–2 arcmin. These data are a powerful probe of both the turbulence and large-scale structure of magneto-ionic gas, and have revealed a variety of new features in the interstellar medium.

November 10, 2018

## INTRODUCTION

The Milky Way was the first celestial radio source discovered, and was subsequently one of the first sources to be detected in linear polarization. There are two sources of this polarization: discrete objects such as supernova remnants (SNRs), and a diffuse polarized background produced by the relativistic component of the interstellar medium (ISM). All of this emission undergoes Faraday rotation as it propagates towards us, either in the source itself or in intervening material. With sufficiently high angular and frequency resolution, we can use the properties of this polarized emission to map out the distribution of ionized gas and magnetic fields in individual sources and in the ambient ISM. Only recently have instruments and techniques advanced to a point where such studies are feasible [9,10,16].

Motivated by the spectacular single-dish polarization surveys of Duncan et al [4,5], we have made polarimetric images of the entire fourth quadrant of the Galaxy

with the Australia Telescope Compact Array (ATCA). These data have been taken as part of the Southern Galactic Plane Survey (SGPS; [12]). While the primary focus of the SGPS is to study the Galactic distribution of H I, the ATCA simultaneously receives full polarimetric continuum data, which have allowed us to map out the distribution of linearly polarized emission in the survey region.

While the full survey has now been completed, a detailed analysis has only been carried out on a 28-deg<sup>2</sup> test region, covering the range  $325.5 < l < 332.5$ ,  $-0.5 < b < +3.5$ . We here summarize the main results of this analysis; this work is described in more detail by Gaensler et al [6].

## OBSERVATIONS AND REDUCTION

The ATCA is a 6-element synthesis telescope, located near Narrabri, NSW, Australia. Observations of the test region of the SGPS were carried out in nine observing runs in 1997 and 1998, and comprised 190 separate telescope pointings (see [12] for details). Data were recorded in nine spectral channels spread across 96 MHz of bandwidth and centered at a frequency of 1384 MHz. The two sources MRC B1438–481 and MRC B1613–586 were observed over a wide range in parallactic angle in order to solve for the instrumental polarization characteristics of each antenna [15]. For each spectral channel, images of the field in Stokes  $I$ ,  $Q$ ,  $U$  and  $V$  were deconvolved jointly using the maximum entropy algorithm PMOSMEM [14] and then smoothed to a resolution of  $\sim 1$  arcmin. The final sensitivity in each image is  $\lesssim 0.5$  mJy beam<sup>-1</sup>.

Images of linearly polarized intensity,  $L = (Q^2 + U^2)^{1/2}$ , linearly polarized position angle,  $\Theta = \frac{1}{2} \tan^{-1}(U/Q)$ , and uncertainty in position angle,  $\Delta\Theta = \sigma_{Q,U}/2L$ , were then formed from each pair of  $Q$  and  $U$  images. The nine  $L$  maps (one per spectral channel) were then averaged together to make a final image of  $L$  for the entire test region, while the nine  $\Theta$  and  $\Delta\Theta$  maps were used to derive an image of the rotation measure (RM) over the field.

## RESULTS

In Figure 1 we show images of  $I$  and  $L$  from both our 1.4-GHz ATCA observations and from the 2.4-GHz Parkes survey of Duncan et al [4] (resolution 10'4). The total intensity images show the presence of SNRs and H II regions (see [12] for further discussion). Although the interferometric ATCA observations are not sensitive to the diffuse emission seen by Parkes, it is clear that the same features are present in both data-sets.

At first glance it seems that the  $L$  images have very little in common with the Stokes  $I$  emission. In particular, the ATCA  $L$  image is dominated by diffuse polarization spread all over the field of view, composed of discrete patches separated by narrow “canals” of reduced polarization. While none of this emission is correlated

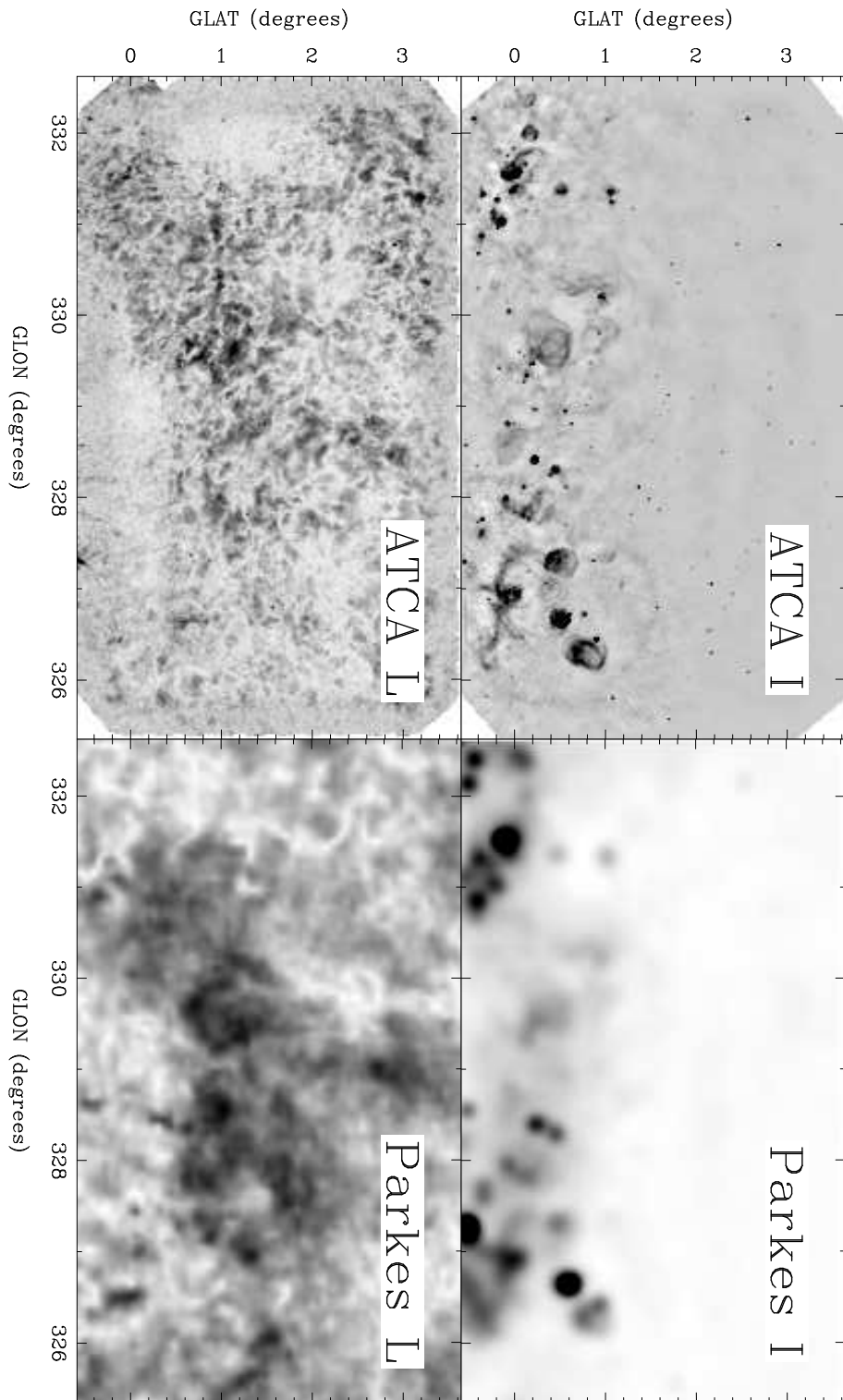


**FIGURE 1.** Images of the SGPS test region with the ATCA (1.4 GHz, 1 arcmin resolution) and Parkes (2.4 GHz, 10.4 arcmin), in both total and linearly polarized intensity.

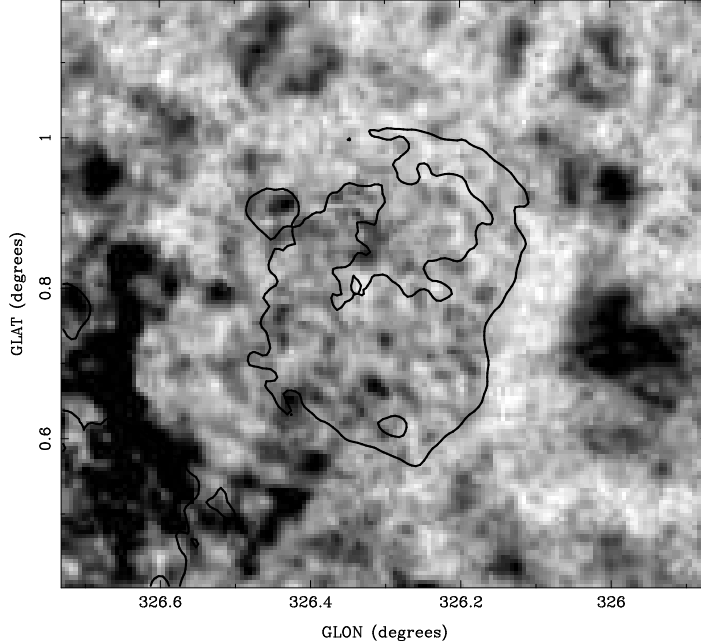


**FIGURE 2.** Polarized emission towards the H II region RCW 94. The greyscale represents linearly polarized intensity, while the single contour corresponds to total intensity emission from the same region at the level of  $45 \text{ mJy beam}^{-1}$ .

with total intensity, there does seem to be a good match between the brightest polarized regions of the ATCA and Parkes data, despite the differing frequencies and resolutions of these data-sets. Using the images of  $\Theta$  and  $\Delta\Theta$ , we can determine the variation of polarization position angle with frequency wherever we detect polarized emission. The resulting RMs are generally small and negative, with a mean RM for the entire field of  $-12.9 \pm 0.1 \text{ rad m}^{-2}$ ; 50% of the RMs have magnitudes smaller than  $\pm 25 \text{ rad m}^{-2}$  and 98% are smaller than  $\pm 100 \text{ rad m}^{-2}$ .

The ATCA  $L$  image reveals two large voids of reduced polarization, each elliptical and several degrees in extent. One void is centered on  $(l, b) = (332^{\circ}.4, +1^{\circ}.4)$  (“void 1”) and the other on  $(328^{\circ}.2, -0^{\circ}.5)$  (“void 2”); both voids are also seen in the 2.4-GHz Parkes polarization map. The RMs around the edges of these voids range up to  $\pm 400 \text{ rad m}^{-2}$ , in distinction to the low RMs seen over the rest of the field.

A careful examination shows one marked correspondence between the ATCA Stokes  $I$  and  $L$  images: at  $(326.3, +0.8)$ , the bright H II region RCW 94 shows reduced polarization towards its interior, and is further surrounded by a halo in which no polarization at all is seen. This is shown in more detail in Figure 2.

Finally, of the numerous unresolved sources distributed across the field, 21 of these sources show detectable linear polarization. The RMs for these sources fall in the range  $-1400 \text{ rad m}^{-2}$  to  $+200 \text{ rad m}^{-2}$ .

# DISCUSSION

## Diffuse Emission

We first note that the incomplete  $u - v$  coverage of an interferometer affects images of polarization in complicated ways. While it is physically required that  $L \leq I$ , and we generally expect that structures seen in  $L$  might correspond to similar structures in  $I$ , neither situation will be generally observed in interferometric data. This is because an interferometer can not detect structures larger than a certain size, corresponding to the closest spacings between its antenna elements (in the case of the ATCA, this maximum scale of  $\sim 35'$ ). A source larger than this maximum scale will not be seen in Stokes  $I$ ; if it is also a uniformly polarized source, it will not be detected in polarization either. However, magnetic field structure within the source, plus variations in the Faraday rotation along different lines-of-sight, can introduce power in Stokes  $Q$  and  $U$  on smaller scales, to which the interferometer is sensitive. We thus can often observe complicated structures in polarization which have no counterpart in total intensity [8–10,16].

Clearly such an effect is occurring here, and is producing virtually all the linear polarization seen in Figure 1. We can crudely divide up the diffuse polarization we see into two components.

The brightest polarization seen with the ATCA matches well the bright polarized structures seen with Parkes. Since the amount of Faraday-induced polarization is very strongly dependent on both resolution and frequency, the fact that two such disparate data-sets show similar structures implies that these bright polarized structures are intrinsic to the emitting regions. By comparing the RMs observed for this emission to those observed for pulsars in this part of the sky, we can conclude that the distance to this emission is in the range 1.3–4.5 kpc. The depolarizing effects of RCW 94 (discussed further below) imply that the polarized emission is  $>3$  kpc distant, while the lack of depolarization against other H II regions gives an upper limit of 6.5 kpc. Dickey [2] has made H I absorption measurements against this emission to derive a lower limit on its distance of 2 kpc. Taking into account all these constraints, we argue that the mean distance to the source of polarized emission is  $3.5 \pm 1.0$  kpc, corresponding to the Crux spiral arm of our Galaxy.

The rest of the ATCA field is filled with fainter diffuse polarization, which does not have any counterpart in the Parkes data. This emission is best explained as being due to Faraday rotation in foreground material. The RMs measured for this emission imply that they are caused by foreground clouds of  $\text{RM} \sim 5 \text{ rad m}^{-2}$ , consistent with the conclusions made by Wieringa et al [16].

## Voids in Polarization

To the best of our knowledge, voids in polarization such as those described here have not been previously reported. There are two possible explanations to account

for these structures: either they represent regions where the level of intrinsic polarization is low, or they are the result of propagation through a foreground object, whose properties have depolarized the emission at both 1.4 and 2.4 GHz.

If the voids are intrinsic to the emitting regions, then the distance of 3.5 kpc inferred above implies that they are hundreds of parsecs across — it is hard to see what could produce such uniformly low polarized intensity across such large regions. We thus think it unlikely that the voids are intrinsic to the emitting regions.

We thus favor the possibility that the voids are caused by depolarizing effects in foreground material. We have considered in detail the various ways in which foreground Faraday rotation can produce the observed structure, and can rule out bandwidth and gradient depolarization as possible mechanisms (see [6] for details).

The only remaining possibility is that depolarization in the voids is due to beam depolarization, in which the RM varies randomly on small scales. We have developed a detailed model for “void 1” to confirm this. We consider void 1 to be a caused by a sphere of uniform electron density  $n_e \text{ cm}^{-3}$ , centered on  $(332^\circ 5, +1^\circ 2)$  with a radius of  $1.4$  and at a distance to us of  $d$  kpc. Within the sphere, we suppose that there are random and ordered components to the magnetic field, and that these two components have identical amplitudes  $B \mu\text{G}$ . The ordered component is uniformly oriented at an angle  $\theta$  to the line of sight. We assume that the random component is coherent within individual cells of size  $l$  pc, but that the orientation from cell to cell is random. Uniformly polarized rays which propagate through a different series of cells will experience differing levels of Faraday rotation, resulting in beam depolarization when averaged over many different paths.

By calculating the properties of the polarized signal which emerges after propagating through this source, we find that we can account for the observed properties of void 1 if  $n_e \sim 20 \text{ cm}^{-3}$ ,  $B \sim 5 \mu\text{G}$ ,  $\theta \gtrsim 80^\circ$ ,  $d \sim 300 \text{ pc}$  and  $l \sim 0.2 \text{ pc}$  (see [6] for details). These properties are consistent with those of an H II region of comparatively low emission measure. Indeed Figure 3 demonstrates that H $\alpha$  emission fills void 1, its morphology and perimeter matching exactly to that of the void. It is interesting to note that the O9V star HD 144695 is very close to the projected center of void 1, and is at a distance of  $300 \pm 160 \text{ pc}$ . The radius of the Strömgen sphere which this star would produce is consistent with the extent of the void. It is thus reasonable to propose that the star is embedded in and powers the surrounding ionized bubble.

Two properties of the voids which our simple model cannot account for are the requirement that the uniform component of the magnetic field be largely oriented in the plane of the sky, but that we generally observe coherent regions of large RM (of the order of a few hundred  $\text{rad m}^{-2}$ ) around the edges of the voids. We suggest that both these results can be explained by the field geometry which arises during the expansion phase of an H II region as it interacts with surrounding material. This produces a magnetic field perpendicular to the line of sight over most of the void, but which is parallel to the line of sight (and can thus potentially produce high RMs) around the perimeter.

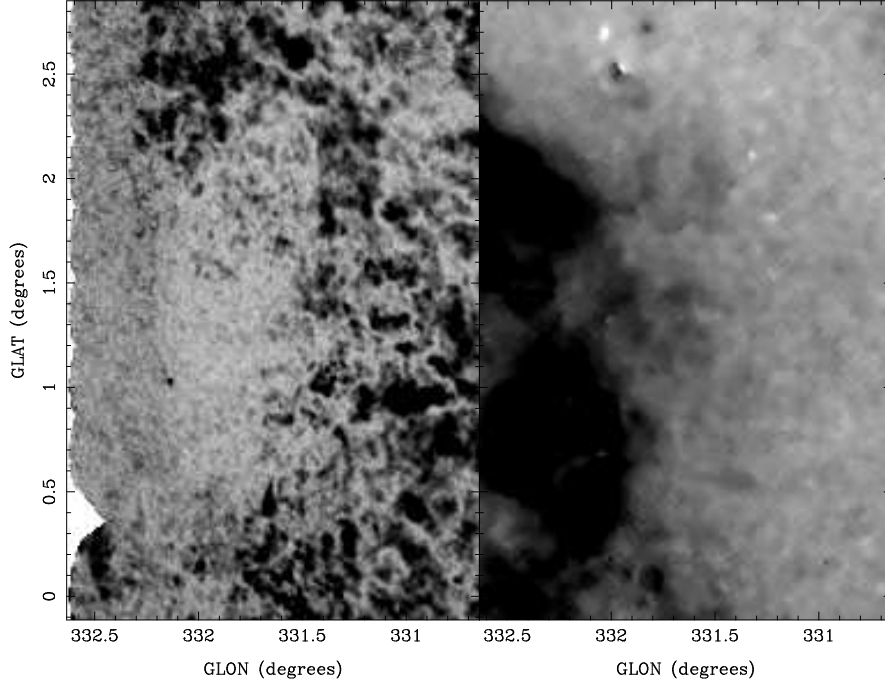


**FIGURE 3.** Comparison of linear polarization (left, [6]) and  $H\alpha$  emission (right, [7]) towards void 1.

## Depolarization seen towards RCW 94

The reduced polarization seen coincident with RCW 94 in Figure 2 presumably results from beam depolarization, just as for the H II region argued to produce void 1. However, the effects of beam depolarization are expected to be weakest around the edges of the source, and thus cannot account for the halo of complete depolarization surrounding RCW 94. We rather account for this depolarization halo by requiring the electron density to be approximately constant across RCW 94, but to fall off rapidly beyond the boundaries of the source. This produces a sharp gradient in RM around the edges of the source, resulting in complete depolarization.

The presence of significant CO emission at the same position and systemic velocity as for RCW 94 [1] suggests that the H II region is interacting with a molecular cloud. This possibility is supported by H I observations of the region, which show that RCW 94 is embedded in a shell of H I emission, which is further surrounded by a ring of decreased H I emission [11]. McClure-Griffiths et al [11,12] argue that this structure in H I confirms that RCW 94 is embedded in a molecular cloud, the shell of emission resulting from  $H_2$  molecules dissociated by the H II region, and the surrounding region of reduced H I corresponding to regions of undisturbed molecular material. Simulations of H II regions evolving within molecular clouds ([13] and references therein) show that for certain forms of the density profile within the parent cloud, the shock driven into the cloud by the embedded expanding H II region can produce a halo of partially ionized material around the latter's perimeter,

which would produce the fall-off in  $n_e$  required to produce the depolarization halo observed.

## Point Sources

With the exception of one source known to be a pulsar, the polarized point sources in our field are presumably extragalactic, and their RMs thus probe the entire line-of-sight through the Galaxy. When combined with information from pulsar RMs, we can use these data to constrain the geometry of the overall Galactic magnetic field. So far we have compared the RMs in our test region to those expected for a bisymmetric spiral configuration, and have found that pitch angles in the lower end of the range allowed by pulsars ( $p \sim -4.5^\circ$ ) are favored [3]. We are in the process of carrying out a more detailed study using the RMs of 163 background sources from the entire SGPS, in which we are comparing these measurements to the distributions expected for a wider variety of geometries and model parameters (Bizunok et al, in preparation).

## CONCLUSIONS

The ATCA's sensitivity, spatial resolution and spectral flexibility have allowed us to study linear polarization and Faraday rotation from the inner Galaxy in an unprecedented detail. Even though the test region we have considered covers less than 7% of the full survey, we have been able to identify a variety of distinct polarimetric phenomena, and have used these to map out both global and turbulent structures in the magneto-ionized ISM. We anticipate that our analysis of the full SGPS will result in a comprehensive study of magnetic fields and turbulence in the inner Galaxy.

## ACKNOWLEDGMENTS

The Australia Telescope is funded by the Commonwealth of Australia for operation as a National Facility managed by CSIRO.  $H\alpha$  data were taken from the Southern H-Alpha Sky Survey Atlas (SHASSA), which is supported by the National Science Foundation. B.M.G. is supported by a Clay Fellowship awarded by the Harvard-Smithsonian Center for Astrophysics, while J.M.D. acknowledges the support of NSF grant AST-9732695 to the University of Minnesota.



## REFERENCES

1. Bronfman, L., Alvarez, H., Cohen, R. S., and Thaddeus, P., 1989, ApJS, 71, 481
2. Dickey, J. M., 1997, ApJ, 488, 258
3. Dickey, J. M., Onken, C. A., McClure-Griffiths, N. M., Gaensler, B. M., Green, A. J., Haynes, R. F., and Wieringa, M. H., in *Radio Polarization: A New Probe of the Galaxy*, edited by T. L. Landecker, Penticton: DRAO, 2001 p. 43
4. Duncan, A. R., Haynes, R. F., Jones, K. L., and Stewart, R. T., 1997, MNRAS, 291, 279
5. Duncan, A. R., Reich, P., Reich, W., and Fürst, E., 1999, A&A, 350, 447
6. Gaensler, B. M., Dickey, J. M., McClure-Griffiths, N. M., Green, A. J., Wieringa, M. H., and Haynes, R. F., 2001, ApJ, 549, 959
7. Gaustad, J. E., McCullough, P. R., Rosing, W., and D., V. B., 2001, Publ. Astr. Soc. Pacific, in press (astro-ph/0108518)
8. Gray, A. D., Landecker, T. L., Dewdney, P. E., and Taylor, A. R., 1998, Nature, 393, 660
9. Gray, A. D., Landecker, T. L., Dewdney, P. E., Taylor, A. R., Willis, A. G., and Normandeau, M., 1999, ApJ, , 221
10. Haverkorn, M., Katgert, P., and de Bruyn, A. G., 2000, A&A, 356, L13
11. McClure-Griffiths, N. M., Dickey, J. M., Gaensler, B. M., Green, A. J., Haynes, R. F., and Wieringa, M. H., 2001, Pub. Astr. Soc. Aust., 18, 84
12. McClure-Griffiths, N. M., Green, A. J., Dickey, J. M., Gaensler, B. M., Green, A. J., Haynes, R. F., and Wieringa, M. H., 2001, ApJ, 551, 394
13. Rodríguez, J. A., Tenorio-Tagle, G., and Franco, J., 1995, ApJ, 451, 210
14. Sault, R. J., Bock, D. C.-J., and Duncan, A. R., 1999, A&AS, 139, 387
15. Sault, R. J., Hamaker, J. P., and Bregman, J. D., 1996, A&AS, 117, 149
16. Wieringa, M. H., de Bruyn, A. G., Jansen, D., Brouw, W. N., and Katgert, P., 1993, A&A, 268, 215